




Structure transition and zigzag magnetic order in Ir/Rh-substituted honeycomb lattice  $\alpha$ -RuCl<sub>3</sub>Zachary Morgan <sup>1</sup>, Iris Ye <sup>2</sup>, Colin L. Sarkis,<sup>1</sup> Xiaoping Wang,<sup>1</sup> Stephen Nagler,<sup>1,3</sup> and Jiaqiang Yan <sup>4</sup><sup>1</sup>Neutron Scattering Division, Oak Ridge National Laboratory, Oak Ridge, Tennessee 37831, USA<sup>2</sup>Next Generation STEM Internship Program Participant at ORNL<sup>3</sup>Department of Physics and Astronomy, University of Tennessee, Knoxville, Tennessee 37996, USA<sup>4</sup>Materials Science and Technology Division, Oak Ridge National Laboratory, Oak Ridge, Tennessee 37831, USA

(Received 17 September 2023; accepted 14 December 2023; published 8 January 2024)

We report magnetization and neutron diffraction studies on crystal and magnetic structures of Ir- and Rh-substituted honeycomb lattice  $\alpha$ -RuCl<sub>3</sub>. The iridium or rhodium atoms are distributed at the Ru site with little structural modification. Both systems undergo a room-temperature monoclinic  $C2/m$  to low-temperature trigonal  $R\bar{3}$  phase transformation with a large recoverable hysteresis. At low temperature, a zigzag spin order is observed with the same characteristic wave vector  $(0,0.5,1)$  as in the parent  $\alpha$ -RuCl<sub>3</sub>. Detailed magnetic structure refinement reveals an ordered moment of  $0.32(5)\mu_B/\text{Ru}$  and an upper boundary of canting angle of  $15(4)^\circ$  away from the basal plane at 5 K for the 10% Ir-substituted  $\alpha$ -RuCl<sub>3</sub>, which is different from the  $0.45\text{--}0.73\mu_B/\text{Ru}$  and  $32^\circ\text{--}48^\circ$  canting angle reported in the parent compound  $\alpha$ -RuCl<sub>3</sub>. The observation of unchanged RuCl<sub>6</sub> local octahedral environment, reduced ordered magnetic moment size and canting angle compared to previously reported highlights the potential to study quantum spin-liquid behavior through nonmagnetic ion doping.

DOI: [10.1103/PhysRevMaterials.8.016201](https://doi.org/10.1103/PhysRevMaterials.8.016201)

## I. INTRODUCTION

The interplay between topology and electron correlation leads to a large variety of interesting topological phenomena in quantum materials. These include fractional quantum Hall effect where the quasiparticles carry a fraction of the electron charge [1,2] and quantum spin liquid (QSL) where the quantum fluctuations prevent magnetic order down to absolute zero temperature [3,4]. The Kitaev spin model on a honeycomb lattice [5] is an exactly solvable example in which spin dynamics fractionalizes into itinerant Majorana fermions and Ising gauge-field excitations. The experimental realization for this model was initially proposed in quasi-two-dimensional (quasi-2D) iridates A<sub>2</sub>IrO<sub>3</sub> [6], where the bond directional Ising interactions arise from the spin-orbit-assisted  $j_{\text{eff}} = 1/2$  state in an edge-sharing environment. Recent focus has gradually shifted to the honeycomb lattice  $\alpha$ -RuCl<sub>3</sub> [7,8]. Despite the appearance of long-range magnetic order at low temperatures, both inelastic neutron scattering and Raman spectroscopy [9–12] have detected a broad scattering continuum in  $\alpha$ -RuCl<sub>3</sub>. This continuum is suggested to align with the predicted presence of itinerant Majorana fermions and is interpreted as indicating that  $\alpha$ -RuCl<sub>3</sub> is proximate to the QSL state. Additionally, anomalous thermal Hall properties are observed in the QSL state with applied in-plane magnetic fields [13–16].

Below  $T_N = 7$  K,  $\alpha$ -RuCl<sub>3</sub> exhibits a zigzag spin structure [17–19] like that observed in honeycomb iridates [20–22]. The static spin configuration is quite fragile and susceptible to various perturbations including in-plane magnetic field [12,23,24], hydrostatic pressure [25–27], stacking disorder [18,28], and chemical substitution [29–34]. In the latter case, partial substitution of Ru<sup>3+</sup> with magnetic Cr<sup>3+</sup> ions

destabilizes the zigzag long-range magnetic order and favors a spin-glass state [31]. Alternatively, the inclusion of nonmagnetic ions such as Rh<sup>3+</sup> [34] and Ir<sup>3+</sup> [29] seems to only suppress the zigzag order without any signature of freezing into a spin-glass state. Furthermore, inelastic neutron scattering studies have found that the key character of fractionalized excitations is maintained in a wide range of Ir concentration even when the long-range spin order is absent [29]. This is particularly intriguing as it reveals the robust nature in the dynamical channel and provides a viable route to achieve the long sought after quantum spin-liquid state in the absence of applied magnetic field.

The impact of chemical substitution on the crystal and magnetic structures of  $\alpha$ -RuCl<sub>3</sub> has not been thoroughly studied before partially due to the unavailability of sizable single crystals. In this work, the growth, magnetic properties, nuclear and magnetic structures of Ru<sub>1-x</sub>R<sub>x</sub>Cl<sub>3</sub> ( $R = \text{Ir, Rh}$ ) single crystals are reported. With a moderate concentration of  $x = 0.1$ , the transition temperature  $T_N$  is suppressed to around 6 K. A large hysteresis about 70 K is present between the room temperature ( $T$ ) monoclinic  $C2/m$  and the low- $T$  trigonal  $R\bar{3}$  crystal structures likely due to the presence of stacking disorder. As observed in  $\alpha$ -RuCl<sub>3</sub>, both systems revert to the room-temperature monoclinic structure after thermal cycling without signs of stacking disorder evident as diffuse scattering along the  $c^*$  axis. A significantly reduced ordered moment of  $0.32(5)\mu_B/\text{Ru}$  is observed in the Ir-substituted  $\alpha$ -RuCl<sub>3</sub> zigzag spin configuration. The spin moment is in the  $ac$  plane with tilting angle  $15(4)^\circ$  away from the  $a$  axis (the direction perpendicular to the Ru-Ru bond). Both the ordered moment size and canting angle are smaller than previous reports in  $\alpha$ -RuCl<sub>3</sub> with moment size of  $0.45\text{--}0.73\mu_B/\text{Ru}$  and canting angle of  $35\text{--}48^\circ$  [17,18].

## II. EXPERIMENTAL DETAILS

Single crystals of Rh- and Ir-substituted  $\alpha$ - $\text{RuCl}_3$  were prepared using self-selecting vapor growth method [35]. The commercial  $\text{RuCl}_3$  powder from Furuya Metals (Japan) was used in the growths without further purification. Pure  $\text{RhCl}_3$  and  $\text{IrCl}_3$  powders were obtained by reacting the transition-metal oxides with  $\text{AlCl}_3$ -KCl salt [36]. Platelike crystals with a typical in-plane dimension of 5–10 mm and thickness up to 1 mm were obtained. Magnetic properties were measured with a Quantum Design (QD) Magnetic Property Measurement System in the temperature range 2.0–300 K. The compositions of the crystals were determined using energy dispersive spectroscopy (EDS) with a Hitachi TM3000 scanning electron microscope and Bruker Quantax70 spectrometer. EDS suggests the transition-metal/chlorine ratio is 1:3. However, the significant overlap of peaks prevents a reliable determination of the real composition. Therefore, nominal composition is used in this work. Magnetic measurements were used to screen crystals for further characterizations. We noticed some variation of magnetic and structural transitions among crystals from the same batch, indicating the variation of substitution content. Therefore, magnetic and neutron diffraction measurements were performed on the same piece of crystals for each composition.

Neutron diffraction experiments of 10% substituted compositions were carried out using the single-crystal diffractometer CORELLI [37] at the Spallation Neutron Source (SNS) to study both the crystal and magnetic structures and the corresponding structural transition. Individual crystals were glued to a thin aluminum plate with superglue adhesive and loaded inside a closed-cycle refrigerator with a base temperature of 5 K. The neutron diffraction data are first collected at 200 K (above the structural transition) with 360 degrees of rotation about the vertical axis. After samples were cooled to base temperature, another full map was collected to investigate the magnetic structure. The crystals were then warmed back to 200 K to probe possible structural change after thermal cycling. During initial cooling and subsequent warming, characteristic Bragg peaks that are unique to the specific space group of the crystal were closely monitored as function of temperature with a ramping rate of 1 K/min.

A similar single-crystal neutron diffraction experiment of 20% Rh-substituted samples was also performed on the TOPAZ diffractometer [38,39] at SNS. Crystals were attached via GE varnish to thin aluminum posts with the monoclinic  $a^*$  axis oriented vertically. Sample temperature was controlled by a Cryomech P415 pulse tube cryocooler and data were collected using sample orientations optimized for coverage with the CRYSTALPLAN software [40]. Data were taken above the structural transition at 250 K as well as below the structural transitions at base temperature of 15 K. Crystals were cooled and heated at a rate of 2 K/min and the transitions were tracked studying the nominal (1,1,3) Bragg peak of the low-temperature  $R\bar{3}$  structure.

## III. RESULTS AND DISCUSSION

The temperature-dependent magnetization of 10% Ru- and Ir-substituted  $\alpha$ - $\text{RuCl}_3$  crystals used for neutron diffraction

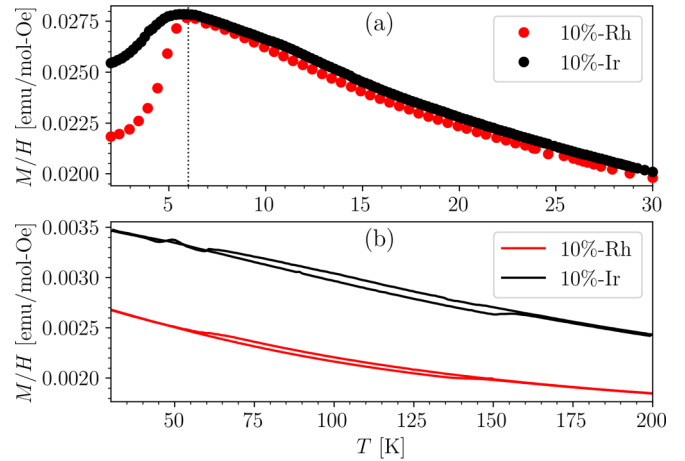


FIG. 1. Temperature dependence of magnetization of 10% Ir- and Ru-substituted  $\alpha$ - $\text{RuCl}_3$ . (a) Low-temperature magnetization highlighting the magnetic ordering temperature. The data were collected in a magnetic field of 1 kOe along an arbitrary direction in *ab* plane. (b) High-temperature magnetization highlighting the structural transition at high temperatures. The measurement is performed with a ramping rate of 2 K/min in a magnetic field of 10 kOe applied perpendicular to the plate.

study at CORELLI is shown in Fig. 1. Both samples exhibit a long-range magnetic order with similar  $T_N = 6$  K. The different magnitudes of the magnetization drop below  $T_N$  may result from different in-plane field directions. A weak hump around 10 K is observed for the Ir-substituted crystals, indicating the presence of stacking disorder in this piece of crystal. The higher-temperature magnetization shown in Fig. 1(b) highlights the structure transition. For both compositions, the transition occurs around 60 K upon cooling and 150 K upon warming, resulting in a wide loop in the temperature-dependent magnetization. In addition, the effective moment obtained from a Curie-Weiss fit to the high-temperature magnetic susceptibility remains around  $2.3 \mu_B/\text{Ru}$ , the same as that of the parent.

The presence of the structure transition is further confirmed by neutron diffraction study. Structural refinement indicates that the substituted  $\alpha$ - $\text{RuCl}_3$  systems crystallize in a monoclinic  $C2/m$  space group at room temperature and transforms to trigonal  $R\bar{3}$  space group at low temperature consistent with other reports in crystals without doping [41,42]. Figure 2(a) shows the  $T$  dependence of the nuclear reflection (1,1,3) indexed in the low- $T$   $R\bar{3}$  space group upon cooling and warming. The abrupt increase in intensity near 75 K of this peak on cooling and sudden disappearance at 150 K on warming confirms the transition is first order and is consistent with previous investigation on the pure  $\alpha$ - $\text{RuCl}_3$  where the temperature difference of the structural transition between cooling and warming critically depends on the degree of stacking disorder [42]. The hysteresis window observed in this study is similar to a previous work with Ir-substituted samples [30]. A narrower hysteresis window typically implies the single crystal contains smaller amounts of stacking disorder. The large hysteresis windows observed in Figs. 1 and 2 might reflect increased stacking disorder. It is yet to be investigated whether

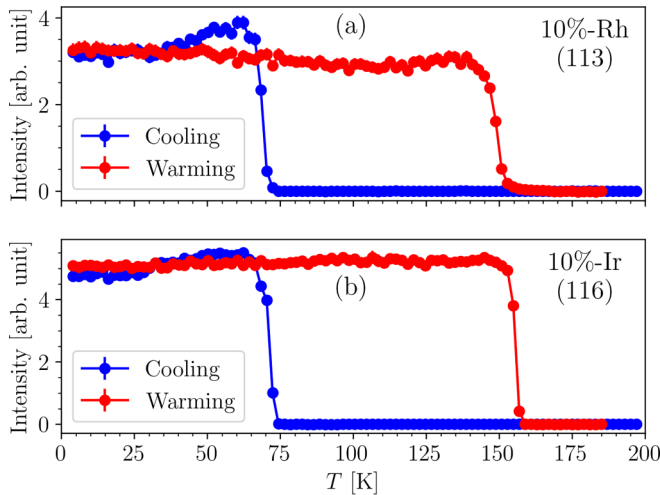


FIG. 2. Cooling (blue) and warming (red) curves of integrated peak intensity for (a) 10% Rh-substituted and (b) 10% Ir-substituted  $\alpha$ - $\text{RuCl}_3$  showing large hysteresis in structure transformation between high-temperature  $C2/m$  monoclinic and low-temperature  $R\bar{3}$  trigonal structure. The first-order transition is complete and does not exhibit remnant phase coexistence at low temperature.

the stacking disorder comes from inappropriate growth parameters or chemical substitution.

In parent  $\alpha$ - $\text{RuCl}_3$ , the structure transition occurs around 170 K upon warming. In contrast, our observations in this study indicate a transition temperature roughly 20 K lower for 10% Rh- or Ir-substituted compositions. This reduction in the structure transition temperature appears to be a consequence of chemical substitution. Figure 3(a) shows the temperature dependence of magnetization of 20% Rh-substituted  $\text{RuCl}_3$ . No long-range magnetic order was observed above 2 K for this composition. The thermal evolution of the (1,1,3) peaks shown in Fig. 3(b) indicates the structure transition

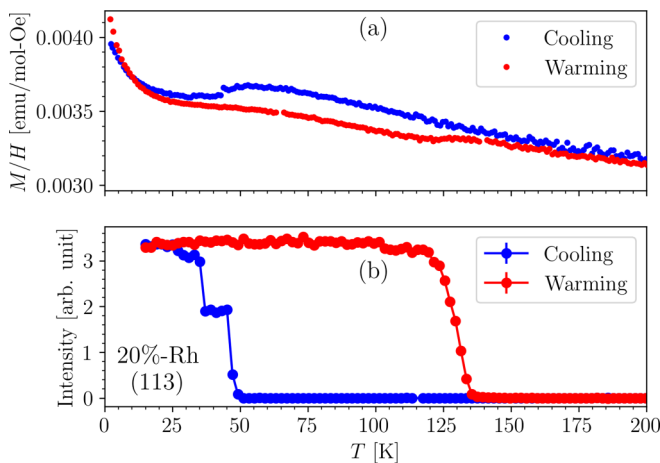


FIG. 3. Temperature dependence of (a) magnetization and (b) intensity of (1,1,3) reflection of 20% Rh-substituted  $\alpha$ - $\text{RuCl}_3$ . Magnetic data were collected with a ramping rate of 2 K/min in a magnetic field of 1 T applied perpendicular the crystal plate. No long-range magnetic order is observed above 2 K while the structure transition is still present.

occurs around 50 K upon cooling and 130 K upon warming. Both temperatures are consistent with those obtained from magnetic measurements. The transition temperature upon warming is further reduced compared to those for 10% Rh or Ir-substituted compositions. This indicates that the nonmagnetic substitution in the honeycomb plane affects not only the in-plane magnetic interactions but also the interlayer coupling. Despite the apparent difference in the thermal hysteresis, the structural parameters among all substituted  $\alpha$ - $\text{RuCl}_3$  samples from structure refinement remain unchanged compared to the parent compound. The lattice constants, bond distances, and bond angles are nearly the same within uncertainty (Supplemental Material [43]). This could be expected as the effective ionic radii of  $\text{Rh}^{3+}$  is 0.665 Å, similar to  $\text{Ir}^{3+}$  and  $\text{Ru}^{3+}$  that are identical at 0.68 Å [44].

The difference between the room-temperature monoclinic  $C2/m$  phase shown in Fig. 4(a) and low- $T$  trigonal  $R\bar{3}$  phase shown in Fig. 4(b) can be visualized in the reciprocal space mappings that are displayed Figs. 4(c)–4(h). Lattice parameter determination from observed structural Bragg peaks indicates room-temperature monoclinic cell parameters with base centering conditions. At low temperature, a hexagonal cell is observed with peaks indexed with rhombohedral centering. Each space group can be confirmed through detailed analysis of the Bragg intensities using least-squares refinement. More details about the structure refinements and Bragg peak integration are given in the Supplemental Material [43]. In the room-temperature phase, the honeycomb layers are stacked in an arrangement corresponding to a simple translation along the  $c$  axis with displacement vector perpendicular to the armchair of the honeycomb bond as illustrated in Fig. 4(a). In the case of the low- $T$  trigonal phase, the stacking sequence is different as shown in Fig. 4(b). Viewing from the direction perpendicular to the basal plane, the neighboring layers are separated by an in-plane displacement vector of  $[2/3a, 1/3a]$ , which is  $60^\circ$  from the armchair bond.

Figures 4(c)–4(h) show the reciprocal space contour maps for both crystals at 200 K (pristine), 5 K (cooled), and 200 K (warmed) conditions. The  $C2/m \rightarrow R\bar{3}$  structural transition induces notable structural diffuse scattering in the low-temperature phase. The line cuts across a Bragg peak along the  $c^*$  direction in Figs. 4(d) and 4(g) for Rh doping and Ir doping, respectively, show clear Lorentzian profile with a full width half-maximum approximately 0.1 reciprocal lattice unit indicating a correlation length of  $155 \pm 5$  Å. However, the samples fully recover the original states after thermal cycling evidenced by the sharp Bragg reflections and the lack of rodlike feature along the  $c^*$  direction. For the crystal with Rh doping, this is shown in Figs. 4(c) and 4(e), which can be compared to the crystal with Ir doping shown Figs. 4(f) and 4(h). Two distinct sets of Bragg intensities are in the low-temperature trigonal phase: one strong and the other weak. The strong set is from the major structural domain, which fulfills the rhombohedral obverse setting ( $-h + k + l = 3n$ ). The weaker set originates from a twinned domain generated by a two-axis rotation about the  $[1, \bar{1}, 0]$  direction of the major domain in the reverse setting ( $h - k + l = 3n$ ). This type of obverse/reverse twinning is common in the  $R\bar{3}$  space group [45]. The population ratio is 77:23. A proper identification of this ratio is important for determining the spin configuration

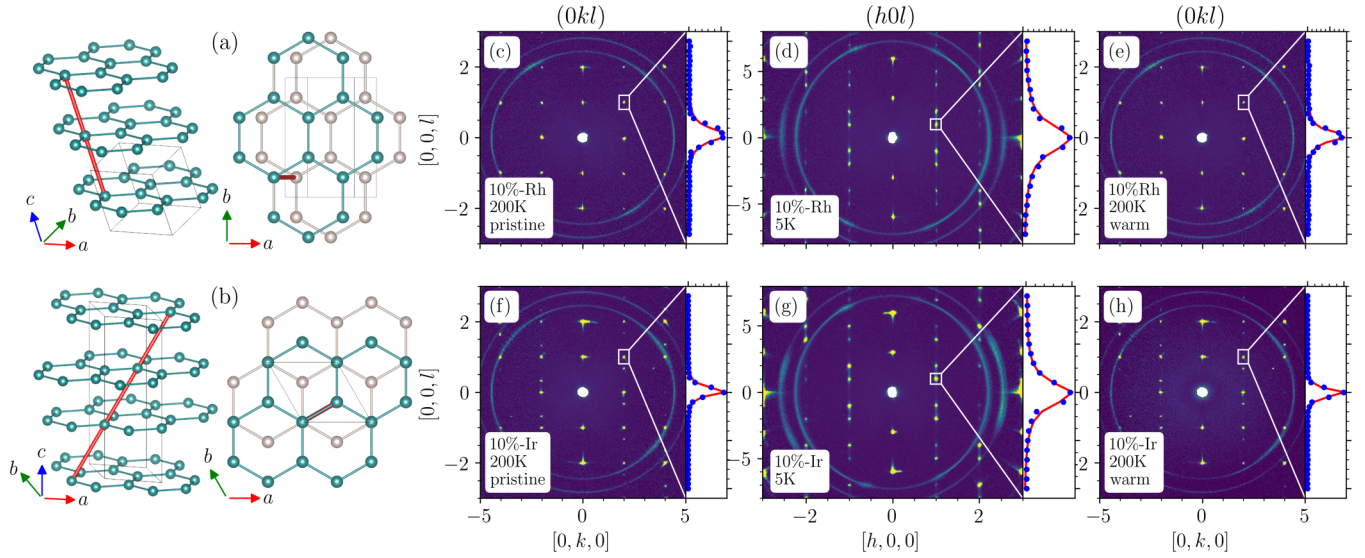


FIG. 4. Stacking sequence of honeycomb layers in (a)  $C2/m$  and (b)  $R\bar{3}$  space groups. The out-of-plane stacking shift vector is  $[0,0,1]$  and  $[2/3, 1/3, 1/3]$ , respectively. Heat map plot of 10% Rh-substituted  $\alpha$ - $\text{RuCl}_3$  at (c) 200 K on first cooling, (d) 5 K, and (e) 200 K after warming. Similar data collected for 10% Ir-substituted  $\alpha$ - $\text{RuCl}_3$  at (f) 200 K on cooling, (g) 5 K, and (h) 200 K on warming. Both Rh- and Ir-substituted crystals are indexed using monoclinic  $C2/m$  space group at high temperature while the low- $T$  data are indexed in the hexagonal  $R\bar{3}$  space group. Note both systems recover to the pristine state showing absence of structural diffuse scattering after thermal cycling back to 200 K. For the Ir-substituted sample, the appearance of an additional domain can be indexed using a twin with  $120^\circ$  rotation about the  $c^*$  axis. This domain recovers after thermal cycling. The inset shows selected line cuts along the  $c^*$  axis with sharp Bragg peaks in the monoclinic phase and broad peaks with diffuse scattering along  $c^*$  in the trigonal setting.

that relies on an accurate account of all structural and magnetic domain contributions.

Both 10% substituted compositions enter a magnetic ordered state at low temperature. The characteristic propagation vector  $(0,0.5,1)$  is the same as that reported in the parent  $\alpha$ - $\text{RuCl}_3$  [17,19] but different from the sample that retains a low- $T$  monoclinic structure [28]. A complete reciprocal space map is necessary to elucidate the coexisting structural and magnetic domains for a reliable determination of the magnetic structure. Figure 5(a) shows the  $(h, k, l = 1)$  slice of the 10% Ir-substituted sample at 5 K. For the major structural domain, there could exist three magnetic twins that are  $120^\circ$  apart along the  $c^*$  axis, since the magnetic wave vector breaks the threefold symmetry. For this domain, two strong magnetic reflections located at  $(0, 0.5, 1)$  and  $(0.5, -0.5, 1)$  are visible and highlighted in closed circles. A third magnetic domain originating from the major structural domain is hardly visible at the expected  $(-0.5, 0, 1)$  peak position. By contrast, the minor structural domain shows one distinct magnetic peak at  $(0, -0.5, 1)$ . Figure 5(b) shows the  $(h = 0, k, l)$  slice where the magnetic satellite peaks are present at  $k = \pm 0.5$ . The line cut along the  $[0, 0, l]$  direction shows markedly strong intensities at  $l = -2, 1, \text{ and } 4$ , while the weak reflections at remaining  $l$  values come from the minor structural domain. The line cut also reveals that the magnetic Bragg peaks from the Ir-substituted sample have similar widths to the structural peaks. Two structural domains are also observed in the 10% Rh-substituted sample at 5 K. The magnetic reflections can also be indexed with the same  $(0, 0.5, 1)$  wave vector, but the magnetic signal is too weak due to lower counting statistics for proper extraction of the magnetic intensities needed for structure refinement. More details related

to 10% Rh-substituted sample are given in the Supplemental Material [43].

The magnetic space group compliant with the wave vector  $(0,0.5,1)$  and Ru ion at the  $6c$  site in the parent  $R\bar{3}$  space group is  $P_5-1$  (#2.7 BNS setting). Although the magnetic cell doubles the unit cell along the  $b$  axis, there is only one magnetic site with  $a$ - and  $c$ -axis components to be determined for the zigzag spin structure. Given that magnetic

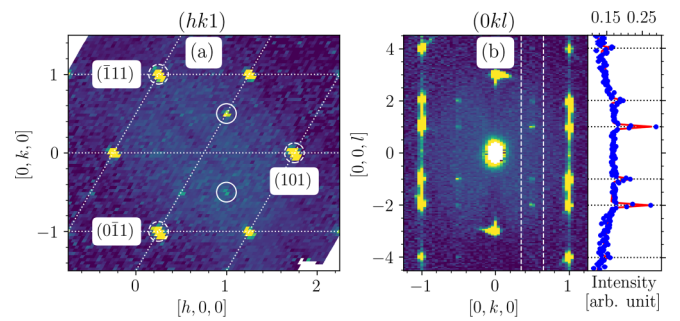


FIG. 5. (a) Intensity slice in the  $(h, k, 1)$  plane showing the magnetic satellite peaks with propagation wave vector  $(0,0.5,1)$  for the 10% Ir-substituted  $\alpha$ - $\text{RuCl}_3$  at  $T = 5.0$  K. Two structural domains correspond to obverse/reverse twinning with volume ratio of 77:23. Structural peaks from the major domain are highlighted in dashed white circles. The magnetic twins associated with the major structural domain are evident with  $120^\circ$  rotation along  $c^*$  and marked in closed white circles and the axes are skewed according to the  $60^\circ$  angle between  $a^*$  and  $b^*$ . (b) The intensity slice in the  $(0, k, l)$  plane. Magnetic reflections are present at  $k = \pm 0.5$  with  $l = \pm 1, \pm 2$  and  $\pm 4$ . The line cut across  $k = 0.5$  shows a distinct distribution of intensities corresponding to the two structural domains.

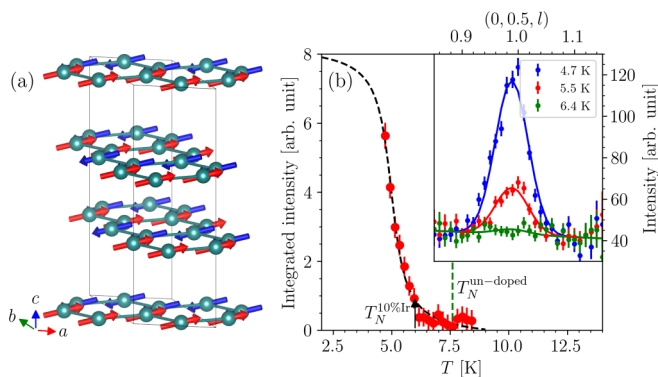


FIG. 6. (a) Refined zigzag spin structure of 10% Ir-substituted  $\alpha$ -RuCl<sub>3</sub> at  $T = 5.0$  K. The magnetic moments are aligned in the  $ac$  plane with a canting angle of  $15(4)^\circ$  away from the basal plane. (b) The temperature dependence of the integrated intensity of the  $(0, 0.5, l)$  magnetic reflection. The dashed line is a guide to eye. The inset shows selective cuts across the magnetic transition.

intensity measurements probe the spin component perpendicular  $\mathbf{S}_\perp$  to the momentum transfer  $\mathbf{Q}$  [ $\mathbf{S}_\perp = \hat{\mathbf{Q}} \times (\mathbf{S} \times \hat{\mathbf{Q}})$ ], a comprehensive examination of out-of-plane  $l$  components in the surveyed magnetic reflections  $(0, 0.5, l = 1 + 3n)$  further constrains the spin canting angles. A sizable intensity at  $l = 4$  implies the spin component is directed closer to the  $ab$  plane. Together with magnetic reflections from other twinned magnetic domains, magnetic structure refinement of the Ir-substituted sample using FULLPROF [46] results in a zigzag structure with spin canting angle slightly away from the basal plane. The goodness of fit remains relatively flat for the canting angle between  $-15^\circ$  to  $15^\circ$  but increases sharply beyond these values. This sets an upper boundary for the canting angle. A more detailed analysis is given in the Supplemental Material [43]. The ordered moment is determined to be  $0.32(5) \mu_B/\text{Ru}$  at 5 K and the resulting spin configuration is illustrated in Fig. 6(a). The thermal evolution of the integrated  $(0, 0.5, 1)$  peak intensity is shown in Fig. 6(b) where the Néel temperature is observed near 6 K and is consistent with the magnetic susceptibility study in Fig. 1(a). An earlier study of pure  $\alpha$ -RuCl<sub>3</sub> [17] reported an ordered moment of  $0.73 \mu_B/\text{Ru}$  at 4 K with canting angle of  $48^\circ$  from the  $a$  axis. The ordered moment at 5 K from this report based on the change in magnetic Bragg peak is estimated to be  $0.69 \mu_B/\text{Ru}$ . In a separate independent study, the ordered moment size at 4.2 K is determined to be  $0.45(5) \mu_B/\text{Ru}$  with canting angle  $35^\circ$  away from the honeycomb plane [18]. This indicates the ordered magnetic moment size of the Ir-substituted  $\alpha$ -RuCl<sub>3</sub> sample observed in this study is smaller than that reported in the parent compound  $\alpha$ -RuCl<sub>3</sub>.

The spin direction is crucial to understand the strength of relative interactions and nature of the zigzag order. Since the discovery of  $\alpha$ -RuCl<sub>3</sub> as one of the promising candidates realizing Kitaev quantum spin liquid, extensive efforts have focused on identifying a proper microscopic model that is capable of capturing the essential features of the inelastic neutron scattering and bulk property data [47–53]. A combined analysis of various experimental observations has converged on a minimal generalized Kitaev-Heisenberg Hamiltonian

$(K-J-\Gamma-\Gamma'-J_3)$  encompassing Ising-like Kitaev interaction  $K$ , Heisenberg exchange  $J$ , symmetric off-diagonal exchange coupling  $\Gamma, \Gamma'$ , and the third-neighbor Heisenberg coupling  $J_3$  [54–61]. The Kitaev term  $K$  for  $\alpha$ -RuCl<sub>3</sub> is generally considered to be ferromagnetic [11,49,55,56] and it is believed the zigzag order is stabilized by either longer-range antiferromagnetic couplings  $J_3$  or anisotropic off-diagonal  $\Gamma$  and  $\Gamma'$  terms [54]. A sufficiently strong anisotropic term  $\Gamma$  leads to a moment locked in the  $ac$ -crystallographic plane while the introduction of  $\Gamma'$ , usually small and originating from trigonal compression, lowers the critical threshold of  $\Gamma$  required to stabilize the moment. The canting angle  $\alpha$  away from the honeycomb plane can be analytically expressed as  $\tan 2\alpha = 4/\sqrt{2}(1+r)/(7r-2)$  where  $r = -\Gamma/(K + \Gamma')$  [22,54]. The canting angle obtained in this study serves as a valuable constraint for understanding the relative strength of the terms  $K, \Gamma,$  and  $\Gamma'$  in further studies of the microscopic models of substituted  $\alpha$ -RuCl<sub>3</sub>.

Furthermore, our structure investigation reveals minimal alteration of the lattice parameters and average local RuCl<sub>6</sub> environment when compared to the parent compound  $\alpha$ -RuCl<sub>3</sub> (see Supplemental Material [43]). The trigonal crystal electric field arising from compression of the RuCl<sub>6</sub> octahedra, plays a pivotal role in stabilizing the zigzag order evidenced from the strong anisotropic magnetization [62], akin to observations in iridates [63]. The absence of significant changes in these structural parameters suggests the suppression of both the transition temperature and ordered moment comes from factors other than chemical pressure [34] or alterations of crystalline electric field. One possible contributing factor could be the disruption of exchange pathways due to the dilution of the honeycomb lattice. On the other hand, the inelastic neutron scattering spectra have shown that the spin-liquid state in Ru<sub>1-x</sub>Ir<sub>x</sub>Cl<sub>3</sub> is robust against iridium doping; the low- $T$  characteristic upper excitation feature associated with the fractionalized excitations is present in a wide range of nonmagnetic iridium doping even when the static spin order is completely absent [29]. This is in line with the recent theoretical study where the introduction of nonmagnetic vacancy concentrations preserves most of the spin-liquid behavior [64]. The vacancies contribute to a pileup of Majorana modes accumulated in the density of states, which can be experimentally verified by future low- $T$  specific heat measurements.

#### IV. SUMMARY

In summary, we use neutron single-crystal diffraction to determine the crystal and magnetic structure of honeycomb lattice  $\alpha$ -RuCl<sub>3</sub> with Ru partially substituted by nonmagnetic Rh<sup>3+</sup> and Ir<sup>3+</sup> ions. Similar to  $\alpha$ -RuCl<sub>3</sub>, both 10% substituted samples exhibit a zigzag magnetic order with an identical characteristic magnetic wave vector below  $T_N$ , undergo a first-order structural transition from room-temperature  $C2/m$  to low-temperature  $R\bar{3}$  phase, fully revert to their original  $C2/m$  state after undergoing thermal cycling. An examination of the nuclear structure suggests that the substitution of Ir/Rh does not introduce any significant alterations in either the average structure or the local environment of the RuCl<sub>6</sub> octahedra. However, both the magnetic order and the structural

transition upon warming are observed to occur at lower temperatures in these chemically substituted samples, indicating the nonmagnetic impurities affect both the in-plane magnetic interactions and the interlayer coupling. The magnetic structure refinement conducted in the Ir-substituted sample has revealed a reduction in both the ordered magnetic moment size and canting angle when compared to the values reported earlier for  $\alpha$ -RuCl<sub>3</sub>. These findings provide valuable constraints for future theoretical investigations into the magnetic Hamiltonian in substituted  $\alpha$ -RuCl<sub>3</sub>. Chemical substitution with nonmagnetic ions of similar atomic radii presents an attractive approach for tailoring the magnetic properties of materials in close proximity to a quantum spin-liquid state.

## ACKNOWLEDGMENTS

I.Y. was supported by the Oak Ridge National Laboratory (ORNL) Next Generation STEM Internship Program (NGSI) Program, sponsored by the U.S. Department of Energy and administered by the Oak Ridge Institute for Science and Education. This research was supported by the U.S. Department of Energy (DOE), Office of Science, National Quantum Information Science Research Centers, Quantum Science Center and used resources at the Spallation Neutron Source, a DOE Office of Science User Facility operated by ORNL. All drawings of crystal and magnetic structures were obtained using VESTA software [65]. This paper has been authored by UT-Battelle, LLC, under Contract No. DE-AC05-00OR22725 with the U.S. Department of Energy.

- 
- [1] X. Du, I. Skachko, F. Duerr, A. Luican, and E. Y. Andrei, Fractional quantum Hall effect and insulating phase of Dirac electrons in graphene, *Nature (London)* **462**, 192 (2009).
- [2] K. I. Bolotin, F. Ghahari, M. D. Shulman, H. L. Stormer, and P. Kim, Observation of the fractional quantum Hall effect in graphene, *Nature (London)* **462**, 196 (2009).
- [3] L. Balents, Spin liquids in frustrated magnets, *Nature (London)* **464**, 199 (2010).
- [4] K. Kitagawa, T. Takayama, Y. Matsumoto, A. Kato, R. Takano, Y. Kishimoto, S. Bette, R. Dinnebier, G. Jackeli, and H. Takagi, A spin-orbital-entangled quantum liquid on a honeycomb lattice, *Nature (London)* **554**, 341 (2018).
- [5] A. Kitaev, Anyons in an exactly solved model and beyond, *Ann. Phys. (NY)* **321**, 2 (2006).
- [6] G. Jackeli and G. Khaliullin, Mott insulators in the strong spin-orbit coupling limit: From Heisenberg to a quantum compass and Kitaev models, *Phys. Rev. Lett.* **102**, 017205 (2009).
- [7] K. W. Plumb, J. P. Clancy, L. J. Sandilands, V. V. Shankar, Y. F. Hu, K. S. Burch, H.-Y. Kee, and Y.-J. Kim,  $\alpha$ -RuCl<sub>3</sub>: A spin-orbit assisted Mott insulator on a honeycomb lattice, *Phys. Rev. B* **90**, 041112(R) (2014).
- [8] H. Takagi, T. Takayama, G. Jackeli, G. Khaliullin, and S. E. Nagler, Concept and realization of Kitaev quantum spin liquids, *Nature Rev. Phys.* **1**, 264 (2019).
- [9] L. J. Sandilands, Y. Tian, K. W. Plumb, Y.-J. Kim, and K. S. Burch, Scattering continuum and possible fractionalized excitations in  $\alpha$ -RuCl<sub>3</sub>, *Phys. Rev. Lett.* **114**, 147201 (2015).
- [10] J. Nasu, J. Knolle, D. L. Kovrizhin, Y. Motome, and R. Moessner, Fermionic response from fractionalization in an insulating two-dimensional magnet, *Nature Phys.* **12**, 912 (2016).
- [11] A. Banerjee, C. A. Bridges, J.-Q. Yan, A. A. Aczel, L. Li, M. B. Stone, G. E. Granroth, M. D. Lumsden, Y. Yiu, J. Knolle, S. Bhattacharjee, D. L. Kovrizhin, R. Moessner, D. A. Tennant, D. G. Mandrus, and S. E. Nagler, Proximate Kitaev quantum spin liquid behaviour in a honeycomb magnet, *Nature Mater.* **15**, 733 (2016).
- [12] A. Banerjee, P. Lampen-Kelley, J. Knolle, C. Balz, A. A. Aczel, B. Winn, Y. Liu, D. Pajerowski, J. Yan, C. A. Bridges, A. T. Savici, B. C. Chakoumakos, M. D. Lumsden, D. A. Tennant, R. Moessner, D. G. Mandrus, and S. E. Nagler, Excitations in the field-induced quantum spin liquid state of  $\alpha$ -RuCl<sub>3</sub>, *npj Quantum Mater.* **3**, 8 (2018).
- [13] Y. Kasahara, T. Ohnishi, Y. Mizukami, O. Tanaka, S. Ma, K. Sugii, N. Kurita, H. Tanaka, J. Nasu, Y. Motome, T. Shibauchi, and Y. Matsuda, Majorana quantization and half-integer thermal quantum Hall effect in a Kitaev spin liquid, *Nature (London)* **559**, 227 (2018).
- [14] T. Yokoi, S. Ma, Y. Kasahara, S. Kasahara, T. Shibauchi, N. Kurita, H. Tanaka, J. Nasu, Y. Motome, C. Hickey, S. Trebst, and Y. Matsuda, Half-integer quantized anomalous thermal Hall effect in the Kitaev material candidate  $\alpha$ -RuCl<sub>3</sub>, *Science* **373**, 568 (2021).
- [15] J. A. N. Bruin, R. R. Claus, Y. Matsumoto, N. Kurita, H. Tanaka, and H. Takagi, Robustness of the thermal Hall effect close to half-quantization in  $\alpha$ -RuCl<sub>3</sub>, *Nature Phys.* **18**, 401 (2022).
- [16] P. Czajka, T. Gao, M. Hirschberger, P. Lampen-Kelley, A. Banerjee, N. Quirk, D. G. Mandrus, S. E. Nagler, and N. P. Ong, Planar thermal Hall effect of topological bosons in the Kitaev magnet  $\alpha$ -RuCl<sub>3</sub>, *Nature Mater.* **22**, 36 (2023).
- [17] S.-Y. Park, S.-H. Do, K.-Y. Choi, D. Jang, T.-H. Jang, J. Schefer, C.-M. Wu, J. S. Gardner, J. M. S. Park, J.-H. Park, and S. Ji, [arXiv:1609.05690](https://arxiv.org/abs/1609.05690).
- [18] H. B. Cao, A. Banerjee, J.-Q. Yan, C. A. Bridges, M. D. Lumsden, D. G. Mandrus, D. A. Tennant, B. C. Chakoumakos, and S. E. Nagler, Low-temperature crystal and magnetic structure of  $\alpha$ -RuCl<sub>3</sub>, *Phys. Rev. B* **93**, 134423 (2016).
- [19] C. Balz, L. Janssen, P. Lampen-Kelley, A. Banerjee, Y. H. Liu, J.-Q. Yan, D. G. Mandrus, M. Vojta, and S. E. Nagler, Field-induced intermediate ordered phase and anisotropic interlayer interactions in  $\alpha$ -RuCl<sub>3</sub>, *Phys. Rev. B* **103**, 174417 (2021).
- [20] S. K. Choi, R. Coldea, A. N. Kolmogorov, T. Lancaster, I. I. Mazin, S. J. Blundell, P. G. Radaelli, Y. Singh, P. Gegenwart, K. R. Choi, S.-W. Cheong, P. J. Baker, C. Stock, and J. Taylor, Spin waves and revised crystal structure of honeycomb iridate Na<sub>2</sub>IrO<sub>3</sub>, *Phys. Rev. Lett.* **108**, 127204 (2012).
- [21] F. Ye, S. Chi, H. Cao, B. C. Chakoumakos, J. A. Fernandez-Baca, R. Custelcean, T. F. Qi, O. B. Korneta, and G. Cao, Direct evidence of a zigzag spin-chain structure in the honeycomb lattice: A neutron and x-ray diffraction investigation of single-crystal Na<sub>2</sub>IrO<sub>3</sub>, *Phys. Rev. B* **85**, 180403(R) (2012).
- [22] J. Chaloupka, G. Jackeli, and G. Khaliullin, Zigzag magnetic order in the iridium oxide Na<sub>2</sub>IrO<sub>3</sub>, *Phys. Rev. Lett.* **110**, 097204 (2013).

- [23] J. A. Sears, Y. Zhao, Z. Xu, J. W. Lynn, and Y.-J. Kim, Phase Diagram of  $\alpha$ -RuCl<sub>3</sub> in an in-plane Magnetic Field, *Phys. Rev. B* **95**, 180411(R) (2017).
- [24] S.-H. Baek, S.-H. Do, K.-Y. Choi, Y. S. Kwon, A. U. B. Wolter, S. Nishimoto, J. van den Brink, and B. Büchner, Evidence for a field-induced quantum spin liquid in  $\alpha$ -RuCl<sub>3</sub>, *Phys. Rev. Lett.* **119**, 037201 (2017).
- [25] B. Wolf, D. A. S. Kaib, A. Razpopov, S. Biswas, K. Riedl, S. M. Winter, R. Valentí, Y. Saito, S. Hartmann, E. Vinokurova, T. Doert, A. Isaeva, G. Bastien, A. U. B. Wolter, B. Büchner, and M. Lang, Combined experimental and theoretical study of hydrostatic He-gas pressure effects in  $\alpha$ -RuCl<sub>3</sub>, *Phys. Rev. B* **106**, 134432 (2022).
- [26] X. Wang, F. Zhu, N. Qureshi, K. Beauvois, J. Song, T. Mueller, T. Brückel, and Y. Su, [arXiv:2304.00632](https://arxiv.org/abs/2304.00632).
- [27] P. Bhattacharyya, L. Hozoi, Q. Stahl, J. Geck, and N. A. Bogdanov, *Phys. Rev. B* **108**, L161107 (2023).
- [28] R. D. Johnson, S. C. Williams, A. A. Haghighirad, J. Singleton, V. Zapf, P. Manuel, I. I. Mazin, Y. Li, H. O. Jeschke, R. Valentí, and R. Coldea, Monoclinic crystal structure of  $\alpha$ -RuCl<sub>3</sub> and the zigzag antiferromagnetic ground state, *Phys. Rev. B* **92**, 235119 (2015).
- [29] P. Lampen-Kelley, A. Banerjee, A. A. Aczel, H. B. Cao, M. B. Stone, C. A. Bridges, J.-Q. Yan, S. E. Nagler, and D. Mandrus, Destabilization of magnetic order in a dilute Kitaev spin liquid candidate, *Phys. Rev. Lett.* **119**, 237203 (2017).
- [30] S.-H. Do, W.-J. Lee, S. Lee, Y. S. Choi, K.-J. Lee, D. I. Gorbunov, J. Wosnitzer, B. J. Suh, and K.-Y. Choi, Short-range quasistatic order and critical spin correlations in  $\alpha$ -Ru<sub>1-x</sub>Ir<sub>x</sub>Cl<sub>3</sub>, *Phys. Rev. B* **98**, 014407 (2018).
- [31] G. Bastien, M. Roslova, M. H. Haghighi, K. Mehlawat, J. Hunger, A. Isaeva, T. Doert, M. Vojta, B. Büchner, and A. U. B. Wolter, Spin-glass state and reversed magnetic anisotropy induced by Cr doping in the Kitaev magnet  $\alpha$ -RuCl<sub>3</sub>, *Phys. Rev. B* **99**, 214410 (2019).
- [32] S.-H. Do, C. H. Lee, T. Kihara, Y. S. Choi, S. Yoon, K. Kim, H. Cheong, W.-T. Chen, F. Chou, H. Nojiri, and K.-Y. Choi, Randomly hopping majorana fermions in the diluted Kitaev system  $\alpha$ -Ru<sub>0.8</sub>Ir<sub>0.2</sub>Cl<sub>3</sub>, *Phys. Rev. Lett.* **124**, 047204 (2020).
- [33] S.-H. Baek, H. W. Yeo, S.-H. Do, K.-Y. Choi, L. Janssen, M. Vojta, and B. Büchner, Observation of a random singlet state in a diluted Kitaev honeycomb material, *Phys. Rev. B* **102**, 094407 (2020).
- [34] G. Bastien, E. Vinokurova, M. Lange, K. K. Bestha, L. T. C. Bohorquez, G. Kreutzer, A. Lubk, T. Doert, B. Büchner, A. Isaeva, and A. U. B. Wolter, Dilution of the magnetic lattice in the Kitaev candidate  $\alpha$ -RuCl<sub>3</sub> by Rh<sup>3+</sup> doping, *Phys. Rev. Mater.* **6**, 114403 (2022).
- [35] J.-Q. Yan and M. A. McGuire, Self-selecting vapor growth of transition-metal-halide single crystals, *Phys. Rev. Mater.* **7**, 013401 (2023).
- [36] J.-Q. Yan, B. C. Sales, M. A. Susner, and M. A. McGuire, Flux growth in a horizontal configuration: An analog to vapor transport growth, *Phys. Rev. Mater.* **1**, 023402 (2017).
- [37] F. Ye, Y. Liu, R. Whitfield, R. Osborn, and S. Rosenkranz, Implementation of cross correlation for energy discrimination on the time-of-flight spectrometer CORELLI, *J. Appl. Crystallogr.* **51**, 315 (2018).
- [38] A. J. Schultz, M. R. V. Jørgensen, X. Wang, R. L. Mikkelsen, D. J. Mikkelsen, V. E. Lynch, P. F. Peterson, M. L. Green, and C. M. Hoffmann, Integration of neutron time-of-flight single-crystal Bragg peaks in reciprocal space, *J. Appl. Crystallogr.* **47**, 915 (2014).
- [39] L. Coates *et al.*, A suite-level review of the neutron single-crystal diffraction instruments at Oak Ridge National Laboratory, *Rev. Sci. Instr.* **89**, 092802 (2018).
- [40] J. Zikovsky, P. F. Peterson, X. P. Wang, M. Frost, and C. Hoffmann, Crystalplan: An experiment-planning tool for crystallography, *J. Appl. Crystallogr.* **44**, 418 (2011).
- [41] S. Mu, K. D. Dixit, X. Wang, D. L. Abernathy, H. Cao, S. E. Nagler, J. Yan, P. Lampen-Kelley, D. Mandrus, C. A. Polanco, L. Liang, G. B. Halász, Y. Cheng, A. Banerjee, and T. Berlijn, Role of the third dimension in searching for Majorana fermions in  $\alpha$ -RuCl<sub>3</sub> via phonons, *Phys. Rev. Res.* **4**, 013067 (2022).
- [42] H. Zhang, M. A. McGuire, A. F. May, J. Chao, Q. Zheng, M. Chi, B. C. Sales, D. G. Mandrus, S. E. Nagler, H. Miao, F. Ye, and J. Yan, [arXiv:2303.03682](https://arxiv.org/abs/2303.03682).
- [43] See Supplemental Material at <http://link.aps.org/supplemental/10.1103/PhysRevMaterials.8.016201> for further details regarding the lattice parameters of both phases, bond distances and angles within the octahedra, and magnetic structure analysis, which includes Refs. [17,18,42,46,66–71].
- [44] R. D. Shannon, Revised effective ionic radii and systematic studies of interatomic distances in halides and chalcogenides, *Acta Cryst A* **32**, 751 (1976).
- [45] R. Herbst-Irmer and G. M. Sheldrick, Refinement of obverse/reverse twins, *Acta Cryst B* **58**, 477 (2002).
- [46] J. Rodríguez-Carvajal, Recent advances in magnetic structure determination by neutron powder diffraction, *Phys. B: Condens. Matter* **192**, 55 (1993).
- [47] K. Ran, J. Wang, W. Wang, Z.-Y. Dong, X. Ren, S. Bao, S. Li, Z. Ma, Y. Gan, Y. Zhang, J. T. Park, G. Deng, S. Danilkin, S.-L. Yu, J.-X. Li, and J. Wen, Spin-wave excitations evidencing the Kitaev interaction in single crystalline  $\alpha$ -RuCl<sub>3</sub>, *Phys. Rev. Lett.* **118**, 107203 (2017).
- [48] S. M. Winter, K. Riedl, P. A. Maksimov, A. L. Chernyshev, A. Honecker, and R. Valentí, Breakdown of magnons in a strongly spin-orbital coupled magnet, *Nature Commun.* **8**, 1152 (2017).
- [49] L. Wu, A. Little, E. E. Aldape, D. Rees, E. Thewalt, P. Lampen-Kelley, A. Banerjee, C. A. Bridges, J.-Q. Yan, D. Boone, S. Patankar, D. Goldhaber-Gordon, D. Mandrus, S. E. Nagler, E. Altman, and J. Orenstein, Field evolution of magnons in  $\alpha$ -RuCl<sub>3</sub> by high-resolution polarized terahertz spectroscopy, *Phys. Rev. B* **98**, 094425 (2018).
- [50] T. Cookmeyer and J. E. Moore, Spin-wave analysis of the low-temperature thermal Hall effect in the candidate Kitaev spin liquid  $\alpha$ -RuCl<sub>3</sub>, *Phys. Rev. B* **98**, 060412(R) (2018).
- [51] P. Lampen-Kelley, S. Rachel, J. Reuther, J.-Q. Yan, A. Banerjee, C. A. Bridges, H. B. Cao, S. E. Nagler, and D. Mandrus, Anisotropic susceptibilities in the honeycomb Kitaev system  $\alpha$ -RuCl<sub>3</sub>, *Phys. Rev. B* **98**, 100403(R) (2018).
- [52] I. O. Ozel, C. A. Belvin, E. Baldini, I. Kimchi, S. Do, K.-Y. Choi, and N. Gedik, Magnetic field-dependent low-energy magnon dynamics in  $\alpha$ -RuCl<sub>3</sub>, *Phys. Rev. B* **100**, 085108 (2019).
- [53] J. A. Sears, L. E. Chern, S. Kim, P. J. Bereciartua, S. Francoual, Y. B. Kim, and Y.-J. Kim, Ferromagnetic Kitaev interaction and the origin of large magnetic anisotropy in  $\alpha$ -RuCl<sub>3</sub>, *Nature Phys.* **16**, 837 (2020).

- [54] J. Chaloupka and G. Khaliullin, Magnetic anisotropy in the Kitaev model systems  $\text{Na}_2\text{IrO}_3$  and  $\text{RuCl}_3$ , *Phys. Rev. B* **94**, 064435 (2016).
- [55] H.-S. Kim and H.-Y. Kee, Crystal structure and magnetism in  $\alpha\text{-RuCl}_3$ : An ab initio study, *Phys. Rev. B* **93**, 155143 (2016).
- [56] S. M. Winter, Y. Li, H. O. Jeschke, and R. Valentí, Challenges in design of Kitaev materials: Magnetic interactions from competing energy scales, *Phys. Rev. B* **93**, 214431 (2016).
- [57] Y. S. Hou, H. J. Xiang, and X. G. Gong, Unveiling magnetic interactions of ruthenium trichloride via constraining direction of orbital moments: Potential routes to realize a quantum spin liquid, *Phys. Rev. B* **96**, 054410 (2017).
- [58] W. Wang, Z.-Y. Dong, S.-L. Yu, and J.-X. Li, Theoretical investigation of magnetic dynamics in  $\alpha\text{-RuCl}_3$ , *Phys. Rev. B* **96**, 115103 (2017).
- [59] C. Eichstaedt, Y. Zhang, P. Laurell, S. Okamoto, A. G. Eguiluz, and T. Berlijn, Deriving models for the Kitaev spin-liquid candidate material  $\alpha\text{-RuCl}_3$  from first principles, *Phys. Rev. B* **100**, 075110 (2019).
- [60] P. A. Maksimov and A. L. Chernyshev, Rethinking  $\alpha\text{-RuCl}_3$ , *Phys. Rev. Res.* **2**, 033011 (2020).
- [61] P. Laurell and S. Okamoto, Dynamical and thermal magnetic properties of the Kitaev spin liquid candidate  $\alpha\text{-RuCl}_3$ , *npj Quantum Mater.* **5**, 2 (2020).
- [62] Y. Kubota, H. Tanaka, T. Ono, Y. Narumi, and K. Kindo, Successive magnetic phase transitions in  $\alpha\text{-RuCl}_3$ : XY-like frustrated magnet on the honeycomb lattice, *Phys. Rev. B* **91**, 094422 (2015).
- [63] H. Gretarsson, J. P. Clancy, X. Liu, J. P. Hill, E. Bozin, Y. Singh, S. Manni, P. Gegenwart, J. Kim, A. H. Said, D. Casa, T. Gog, M. H. Upton, H.-S. Kim, J. Yu, V. M. Katukuri, L. Hozoi, J. van den Brink, and Y.-J. Kim, Crystal field splitting and correlation effect on the electronic structure of  $\text{A}_2\text{IrO}_3$ , *Phys. Rev. Lett.* **110**, 076402 (2013).
- [64] W.-H. Kao, J. Knolle, G. B. Halász, R. Moessner, and N. B. Perkins, Vacancy-induced low-energy density of states in the Kitaev spin liquid, *Phys. Rev. X* **11**, 011034 (2021).
- [65] K. Momma and F. Izumi, VESTA 3 for three-dimensional visualization of crystal, volumetric and morphology data, *J. Appl. Cryst.* **44**, 1272 (2011).
- [66] T. M. Michels-Clark, A. T. Savici, V. E. Lynch, X. Wang, and C. M. Hoffmann, Expanding Lorentz and spectrum corrections to large volumes of reciprocal space for single-crystal time-of-flight neutron diffraction, *J. Appl. Cryst.* **49**, 497 (2016).
- [67] V. F. Sears, Neutron scattering lengths and cross sections, *Neutron News* **3**, 26 (1992).
- [68] C. W. Dwiggin, Rapid calculation of X-ray absorption correction factors for spheres to an accuracy of 0.05%, *Acta Cryst. A* **31**, 395 (1975).
- [69] O. Arnold *et al.*, Mantid-Data analysis and visualization package for neutron scattering and  $\mu$  SR experiments, *Nucl. Instrum. Meth. Phys. Res. A* **764**, 156 (2014).
- [70] P. J. Becker and P. Coppens, Extinction within the limit of validity of the Darwin transfer equations. II. Refinement of extinction in spherical crystals of  $\text{SrF}_2$  and  $\text{LiF}$ , *Acta Cryst. A* **30**, 148 (1974).
- [71] V. Petříček, L. Palatinus, J. Plášil, and M. Dušek, Jana2020—a new version of the crystallographic computing system Jana, *Zeitschrift für Kristallographie - Crystalline Mater.* **238**, 271 (2023).